■ **Electro, Physical & Theoretical Chemistry**

Facile Synthesis of Polyhedral Pd Nanocrystals as a Highly Active and Methanol-Tolerant Electrocatalyst for Oxygen Reduction

Yikui Zeng,[a] SiSi Tian,[a] Dongsheng Wang,[a] Hailin Dong,*[b] Xiaoyang Cheng,[a] Yanchun Zhao,*[a] Jianniao Tian,[a] and Xiulin Yang*[a]

The polyhedral Pd nanocrystals are synthesized by a facile conventional hydrothermal method, in which the cetyltrimethylammonium bromide, Fe^{3+} and formaldehyde are designed as structural orientation, etching and reduction agents, respectively. The crystal and morphological characteristics show that the crystal facets of (111) and (220) planes are exposed on the surface of face-centered cubic crystal structure of Pd polyhedron. Electrochemical analyses indicate that the polyhedral Pd/XC-72 catalyst shows the highest electrochemically active surface area ($57.6 \, m^2 \, g^{-1}$), similar half-wave potential and diffusion-limiting current density ($-4.79 \, mA \, cm^{-2}$) with state-of-the-art commercial Pd/C in alkaline electrolytes. The excellent electrocatalytic activity supports a four-electron-transfer pathway and smaller Tafel slope ($67.2 \, mV \, dec^{-1}$) reveals a higher intrinsic activity for ORR. Additionally, the polyhedral Pd/XC-72 catalyst also exhibits much better methanol tolerance crossover effects and long-term stability than commercial Pd/C. All these excellent electrocatalytic performances are considered to be the coaction of the exposed high surface energy facets and more of active sites on the polyhedral crystals surface, which could significantly improve the adsorption and activation energies with oxygenated intermediates in alkaline solution. This work provides a new prospect in designing high active, non-easy tolerance and more stable Pd-based catalyst in alkaline fuel cells.

Introduction

Sluggish kinetics of oxygen reduction reaction (ORR) and methanol crossover effects are two most important barriers that dramatically decrease the electrochemical activity, powder density and faradaic efficiency in direct methanol fuel cells (DMFCs).[1,2] At present, Pt-based catalysts are the most common electrode materials for DMFCs, and Pt has become the main bottleneck for widely practical application of the DMFCs due to its high cost and scarcity.[3,4] Therefore, it is urgent to develop an alternative catalyst replacing expensive Pt for ORR with much cheaper price, higher ORR activities, and better methanol-tolerance ability.[5,6] To overcome the limitations of expensive Pt-based electrocatalysts, Pd-based catalysts have recently attracted much more attention due to its lower cost combined with closing to the state-of-art Pt for ORR in alkaline solution.[7–9]

Over past few decades, numerous efforts have been devoted to construct high electroactive Pd-based ORR catalysts by manipulation of the geometry and electronic structures,[10–12] formation of multi-metal alloy catalysts,[13–15] metal oxide promoted hybrid catalysts,[16,17] and anchoring on support substrate.[18–20] Among these strategies, designing of special geometry and electronic structures of Pd has attracted a wide attention because that the tailored nanocrystals enclosed by specific crystal facets could intrinsically increase the activity and selectivity for reactions such as nanowires,[21,22] concave nanocubes,[23,24] nanotetrapods,[25,26] nanoflowers,[27,28] nanodendrites,[29] and spheres,[30] etc. Generally, the special structures of synthesized materials are greatly affected by changing the surface energy from selective adsorption capping agent and controlling the growth rate of the crystals in the synthesis process.[31] Xia et al. reported the polyhedral Pd nanocrystals using PVP as capping agent, and they found that the exposed Pd (100) facets catalyst supported much higher electrocatalytic activity than Pd (111) facets in acid solution for formic acid electrooxidation.[32] Lu et al. reported that the CTAB assisted synthesis of Pd dendritic nanocrystals enclosed by Pd (111) facets exhibiting a high electrochemical activity and stability for formic acid oxidation.[33] Hoshi and co-workers described the facet-dependent Pd crystals for electrocatalytic ORR, and the results revealed that the activity of them were in the order of Pd (110) < Pd (111) < Pd (100) in acid media.[34] However, the related polyhedral Pd-based catalysts for alkaline ORR are rarely reported so far, and to our knowledge, almost no work has been observed to reveal its intrinsic affecting factors for

[a] Y. Zeng, S. Tian, D. Wang, X. Cheng, Prof. Y. Zhao, Prof. J. Tian, Prof. X. Yang
Key Laboratory for the Chemistry and Molecular Engineering of Medicinal Resources (Ministry of Education of China), College of Chemistry and Pharmacy, Guangxi Normal University, Guilin 541004, P.R. China.
E-mail: xiulin.yang@kaust.edu.sa
yanchunzhao@aliyun.com
[b] Dr. H. Dong
Catalysis and Chiral Technologies (CCT), Johnson Matthey (Shanghai) Catalyst Co. Ltd., Shanghai 201613, P.R. China.
E-mail: donghl1980@126.com

Supporting information for this article is available on the WWW under https://doi.org/10.1002/slct.201701472

electrocatalysis, thus there is an urgent demand to develop a high efficient polyhedral Pd catalyst for ORR in alkaline solution.

In this work, we report a facile and efficient one-step conventional hydrothermal method synthesizing polyhedral Pd nanocrystals with CTAB, $FeCl_3$, and formaldehyde as capping, etching and reduction agents, respectively. The formed polyhedral Pd nanocrystal with an average particle size is about 43.8 nm and crystals surface are enclosed by (111) and (220) facets. In addition, lots of defects are clearly observed on the synthesized polyhedral Pd crystals. The resulted polyhedral Pd/XC-72 catalyst exhibits higher electrochemical ORR activity than the Pd/XC-72 synthesized by sole addition of $FeCl_3$ or CTAB, respectively. Moreover, the polyhedral Pd/XC-72 catalyst also demonstrates excellent methanol-tolerance ability and long-term stability.
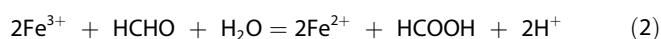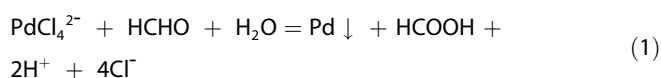
Results and Discussion

Synthesis of polyhedral Pd nanocrystals

The synthetic principle of polyhedral Pd nanocrystals is presented in Scheme 1, in which the precursors of $FeCl_3$,
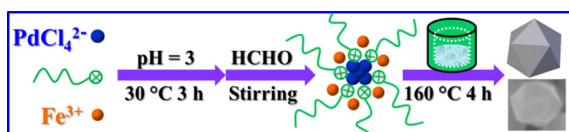
Scheme 1. Schematic description of the synthetic process of polyhedral Pd nanocrystals.

H_2PdCl_4 and CTAB were added into a beaker and adjusted the pH to 3.0 in water bath at 30 °C via one-pot method, and then the reducing agent of HCHO was added under continuous stirring conditions. It is considered that the negatively charged $PdCl_4^{2-}$ ions could initially self-assemble onto the positively charged surfactants of CTAB combined with the oxidizing Fe^{3+} and reductive HCHO in the mixture solution. With increasing the reaction temperature, the oxidizing Fe^{3+} will be slowly reduced to Fe^{2+}, meanwhile, the $PdCl_4^{2-}$ will be reduced to metal Pd crystal seeds. The proposed reaction processes are depicted as **Equations (1) and (2)**. It is believed that the co-existed Fe^{2+}/Fe^{3+} and CTAB could further orientate growth of Pd nanocrystals for polyhedral structures under higher temperature.

$$PdCl_4^{2-} + HCHO + H_2O = Pd \downarrow + HCOOH + 2H^+ + 4Cl^- \tag{1}$$

$$2Fe^{3+} + HCHO + H_2O = 2Fe^{2+} + HCOOH + 2H^+ \tag{2}$$

Crystal structures, morphologies and chemical states analysis

The crystal structures of the as-prepared polyhedral Pd nanocrystal together with Pd/XC-72 (without addition of Fe^{3+} and CTAB) and commercial Pd/C were further detected by XRD as shown in Figure 1A. The characteristic diffraction pattern of
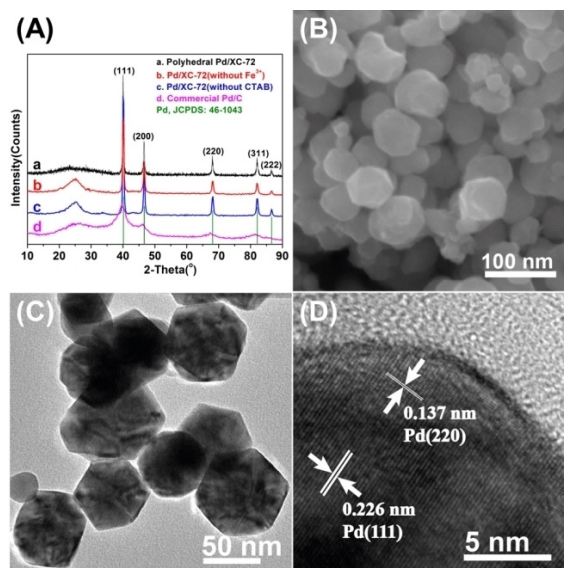
Figure 1. (A) XRD patterns of as-made polyhedral Pd/XC-72, Pd/XC-72(without Fe^{3+}), Pd/XC-72(without Fe^{3+}) and commercial Pd/C. (B) SEM image of polyhedral Pd nanocrystals. TEM image (C) and high-resolution TEM image (D) of polyhedral Pd nanocrystals.

polyhedral Pd/XC-72 exhibits five labeled peaks at $2\theta = 40.05°$, $46.63°$, $68.12°$, $82.05°$ and $86.57°$, corresponding to the (111), (200), (220), (311) and (222) planes of Pd with a face centered cubic (fcc) structure and the space group for *Fm3 m*, respectively, (JCPDS 46–1043).[35] It is observed that the diffraction patterns of Pd/XC-72 (without addition of Fe^{3+} or CTAB) are similar with those of the polyhedral Pd/XC-72 composite. In contrast, the diffraction pattern of commercial Pd/C is much weaker and broader than that of the catalyst we prepared indicating that the crystallinity of Pd in commercial Pd/C is not too high and the particle sizes is also smaller than that of the synthesized three catalysts. Generally, it is believed that the crystal structure, crystallinity and particle sizes will directly co-affect the electrocatalytic activity of the designed catalyst.[36] In addition, the particle size of polyhedral Pd was estimated by analyzing the diffraction peak of Pd (111) using Scherrer formula,[37] and the average particle size is about 43.8 nm.

Figure 1**B** shows the typical SEM image of as-prepared polyhedral Pd nanocrystals. Polyhedral Pd nanocrystals are enclosed by several polygon faces, and the average particle size is 43.5 nm, which is consistent with the calculated results of XRD. As shown in Figure 1**C**, the TEM image of polyhedral Pd nanocrystals exhibits a whole hexagonal structure which can be further split into several secondary triangle faces. It is worth

noted that the uneven dark and light characteristics indicate that there may be a lot of defects in the synthesized polyhedral Pd crystals. The representative high-resolution TEM image (Figure 1**D**) of polyhedral Pd nanocrystals clearly presented some ordered lattice stripes with lattice spacing for 0.226 and 0.137 nm which are in agreement with the (111) and (220) facets of Pd, respectively. Generally, the surface energy of the Pd (220) is much larger than that of the Pd (111) facet, thus, it's could be expected that the Pd (220) facet has much higher activity to adsorb and reduce O_2 molecules.[38] In order to explore the influence of synthesis reagents on the morphologies of polyhedral Pd nanocrystals, only CTAB or $FeCl_3$ was introduced and synthesized different types of Pd particles under similar experimental conditions. When using NaCl instead of $FeCl_3$, the generated particles are identified with different shapes, such as sphere, triangle, square and hexagonal structures (see supporting **Figure S1A**). The formed uneven Pd particles have a wide particle size distribution and are identified between 20 nm and 60 nm. Similarly, when the CTAB was not introduced into the precursors and others kept intact, the resulted products were analyzed with irregular particles and the average particle size of Pd was much smaller than that of the synthesized polyhedral Pd crystals (see supporting **Figure S1B**). These results indicate that polyhedral Pd crystals are only well-formed in the presence of CTAB and Fe^{3+}, in which the formed CTAB-$PdCl_4^{2-}$ complexes were slowly reduced by formaldehyde and formation of Pd seeds in the initial step. Then with the presence and interference by Fe^{3+}/Fe^{2+} and some crystal facets selective adsorption of Br^-,[39] which could lead to a significant difference on the growth rate for Pd crystal surfaces, thus resulting in a specific hexagonal profile structure.

The electronic structure and valence states of the as-prepared catalyst are analyzed by X-ray photoelectron spectroscopy (XPS). **Figure S2**A is the full survey of polyhedral Pd/XC-72, indicating the existence of C, O and Pd in the composite. The deconvoluted C 1s reveals three fitted peaks at binding energies of 284.0 eV, 284.8, 286.0, 288.2 eV which are assigned to C≡C, C—C, C—O and C≡O, respectively (see Figure 2A). The coexistence of different valences of Pd in polyhedral Pd/XC-72 catalyst can be found in the XPS patterns (see Figure 2**B**). By using a Gaussian fitting method, the intense doublet peaks at 334.5 and 339.8 eV, respectively are assigned to metallic Pd^0 and the other two peaks at 335.4 and 340.6 eV are ascribed to Pd^{2+} species.[40,41] Furthermore, the relative peak area of Pd^0 in polyhedral Pd crystals is about 70.3% of the total by measuring the relative peaks. The small proportion of Pd^{2+} might be resulted from the strong interactions between the fresh generated metal Pd and oxygen in the air.[42] Moreover, it should specially note that the Fe 2p was not checked in the composite materials, which indicates that there was no Fe element residue in the synthesized polyhedral Pd crystals (see **Figure S2B**).

Electrochemical performance analysis

Figure 3**A** displays the cyclic voltammograms (CV) of the polyhedral Pd/XC-72, Pd/XC-72 (without Fe^{3+}), Pd/XC-72 (with-
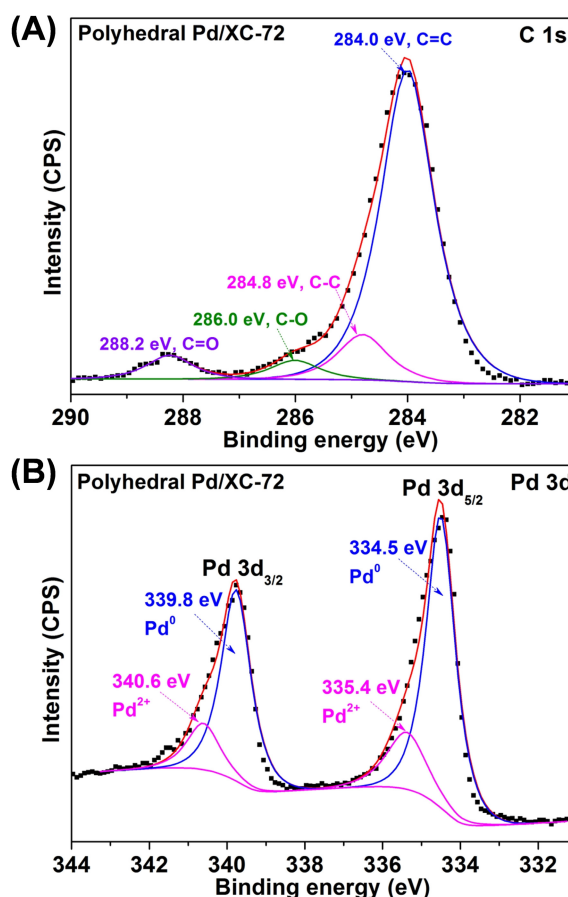

Figure 2. High-resolution XPS spectrum of (A) C 1s and (B) Pd 3d from polyhedral Pd/XC-72 composite.

out CTAB) and commercial Pd/C in an O_2-saturated 0.1 M KOH solution respectively. As shown in the CV curves, the oxidation potential of metal Pd and subsequent well-defined PdO reduction peaks are obtained in the range of -0.5 to 0.1 V. It is worth noted that the reduction peak potential of the polyhedral Pd/XC-72 is -0.220 V, which is obviously much more positive than that of the Pd/XC-72 (without Fe^{3+}, -0.232 V) and commercial Pd/C (-0.235 V) indicating that the formed PdO in polyhedral Pd crystals are much more convenient to be reduced than others. Although the reduction peak potential of polyhedral Pd is slightly more negative than that of Pd/XC-72 (without CTAB), the onset reduction potential of polyhedral Pd is much higher than that of the Pd/XC-72 (without CTAB). All those information reveals that polyhedral Pd crystal surface has weaker chemical adsorption energy for oxygenated substance, which could lead to the surface of Pd continuously generating active sites for favoring high-activity ORR.[43,44] It is well-known that more of active sites could support a better catalytic performance, and the numbers of active sites is proportional to the electrochemically active surface area (EASA).[45] Generally, the reduction peak area of PdO from CV curve is used to calculate the EASA value, and it could be described by the following equation:[46]
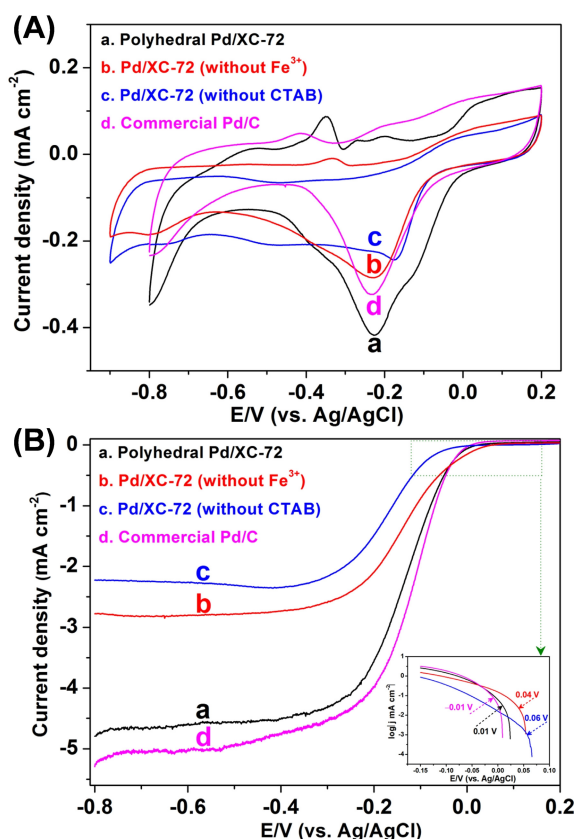
Figure 3. (A) CV curves at a scan rate of 50 mV s^{-1} and (B) ORR polarization curves at a scan rate of 10 mV s^{-1} with a rotating speed for 1600 rpm for different catalysts are conducted in the potential range of 0.2 to -0.8 V in O$_2$-saturated 0.1 M KOH solution. The inset in B is the graph of log|j mA cm^{-2}| versus potential (V).

Where Q is the required charge for the reduction of PdO, S is the required amount of charge for the reduction of the unit area of a single layer of PdO (405 μC cm^{-2}), L is the loading amount of Pd on the electrode. The EAS values of the polyhedral Pd/XC-72 and commercial Pd/C are calculated to be 57.6 and 47.2 m^2 g^{-1}, respectively, which imply that the polyhedral Pd/XC-72 catalyst has more active sites and thus supports better electrochemical ORR activity.

To further investigate ORR electrocatalytic process, the reaction kinetics was analyzed by polarization curves which were performed in O$_2$-saturated 0.1 M KOH solution at a rotating speed of 1600 rpm with a scan rate of 10 mV s^{-1}. As shown in Figure 3**B**, the ORR polarization curves of various catalysts could be roughly divided into three regions: kinetically controlled region (*ca.* 0.1 V ~ -0.2 V), kinetic-diffusion mixing controlled region (*ca.* -0.2 V ~ -0.4 V) and mass diffusion controlled region (lower than -0.4 V).[47,48] In the kinetically controlled regions, it can be found that the onset potential of polyhedral Pd/XC-72 (0.01 V) is higher than that of the commercial Pd/C (-0.01 V), but highly lower than the Pd/XC-72 (without Fe^{3+}, 0.04 V) and Pd/XC-72 (without CTAB, 0.06 V) (see **insert of** Figure 3**B**). Meanwhile, the half-wave potential of polyhedral Pd/XC-72 (-0.134 V) is very close to the commercial

Pd/C (-0.128 V), but more positive than the compared Pd/XC-72 (without Fe^{3+}, -0.141 V), Pd/XC-72 (without CTAB, -0.173 V) and commercial Pt/C (-0.157 V) (see **Figure S3**). In the mass diffusion controlled regions, it is shown that the ORR diffusion-limiting current density of polyhedral Pd/XC-72 (-4.79 mA cm^{-2}) is much higher than those of Pd/XC-72 (without Fe^{3+}, -2.78 mA cm^{-2}) and Pd/XC-72 (without CTAB, -2.22 mA cm^{-2}). In order to better highlight the superiority of our synthesized catalyst, various ever reported Pd-based ORR catalysts have been analyzed and summarized in **Table S1**. The greatly improved electrocatalytic performance of polyhedral Pd/XC-72 could be ascribed to the coaction of high surface energy facet of Pd (220) and the dense defects on the surface of Pd crystals, which could preferentially enable the hydroxyl group to adsorb on its surface for more quickly adsorption/desorption behavior, thus exhibiting excellent ORR electrocatalytic activity combined with more positive applied potential.[49–51]

Figure 4**A** displays the LSV curves of polyhedral Pd/XC-72 in O$_2$-saturated 0.1 M KOH solution at different rotating speed with a scan rate of 10 mV s^{-1}. Based on the Koutecky–Levich (K–L) equation from the mass diffusion controlled region, a series of K–L points can be obtained by the linear relation between the 1/j (the reciprocal of the current density) and ω$^{1/2}$ over a range of potentials:[3]

$$1/j = 1/j_L + 1/j_K \qquad (4)$$

$$j_K = 0.62nFC_0(D_0)^{2/3}v^{-1/6}\omega^{1/2} \qquad (5)$$

where *j*, *j*$_K$ and *j*$_L$ are the measured current density, kinetic- and diffusion limiting current densities, respectively, n is the number of electrons transferred, F is Faradic constant (F = 96485 C mol^{-1}), D$_0$ is the diffusion coefficient of oxygen (D$_0$ = 1.9 × 10^{-5} cm^{-2} s^{-1}), ν is the kinematic viscosity of electrolyte (ν = 1.13 × 10^{-2}), ω is the rotating speed of rotating disk electrode, C$_0$ is the concentration of O$_2$ in saturated solution (C$_0$ = 1.2 × 10^{-3} mol L^{-1}). As show in supporting **Figure S4**, the K–L plots of polyhedral Pd/XC-72 exhibits a good linearity in the range of -0.4 V to -0.6 V. The five fitting lines show similar slopes, which indicates that the electron transfer numbers at the five selected potentials are similar with each other. Similarly, the polarization curves and K–L plots of other compared catalysts are also analyzed and listed in supporting **Figure S5** to **S7**. As shown in Figure 4**B**, the electron transfer numbers of polyhedral Pd/XC-72 (3.52~3.64) are apparently larger than the compared Pd/XC-72 (without Fe^{3+}, 3.03) and Pd/XC-72 (without CTAB, 2.47-2.51), but slightly lower than the commercial Pd/C (3.82-3.94). The result indicates that polyhedral Pd/XC-72 catalyst undergoes a four-electron-transfer pathway dominated for ORR.[52,53]

To better understanding the mechanism of prepared catalysts for ORR, the kinetic current densities of all catalysts are analyzed from the K–L plots and summarized in Figure 4**C**.[54] It can be seen that the kinetic current density of polyhedral Pd/XC-72 is 40.5 mA cm^{-2} at -0.4 V, which is 6.25-, 10.95- and 1.62-fold higher than Pd/XC-72 (without Fe^{3+}), Pd/XC-72 (without CTAB) and commercial Pd/C, respectively. With
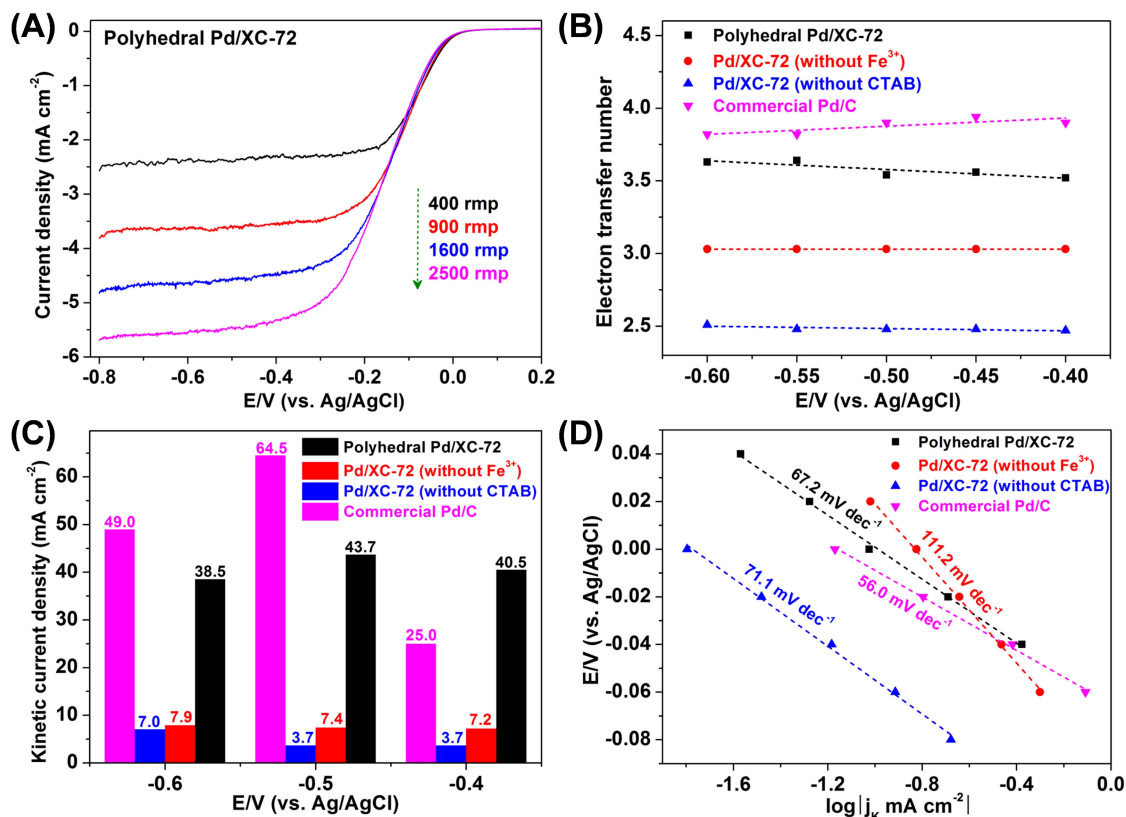
Figure 4. (A) ORR polarization curves of polyhedral Pd/XC-72 catalyst in O_2-saturated 0.1 M KOH at a scan rate of 10 mV s^{-1} with different rotating speeds. Summarized (B) electron transfer numbers between -0.4 and -0.6 V, (C) kinetic current densities from -0.4 to -0.6 V, and (D) Tafel plots for polyhedral Pd/XC-72, Pd/XC-72 (without Fe^{3+}), Pd/XC-72 (without CTAB) and commercial Pd/C, respectively.

increasing the applied potential to 0.5 V and 0.6 V, the kinetic current density of commercial Pd/C is slightly higher than polyhedral Pd/XC-72, which may be due to the smaller particle size of Pd supporting better contacted with the diffusion solution.

The Tafel slopes of all the catalysts are also used to evaluate the kinetic ORR features as shown in Figure 4**D**. The polyhedral Pd/XC-72 presents a Tafel slope for 67.2 mV dec^{-1}, indicating that the first electron transfer on the catalyst is the rate-determining step for the adsorption of intermediates.[55] This vale is close to the commercial Pt/C catalyst (56.0 mV dec^{-1}), revealing that the polyhedral Pd/XC-72 has a higher intrinsic activity for ORR.

Tolerance to methanol and stability evaluation

The methanol crossover on cathode catalyst is an important issue causing wide attention in the application of fuel cells, especially for the noble metal-based catalyst. In this case, the methanol crossover effects on different catalysts are detailly evaluated by the LSV measurements in O_2-saturated 0.1 M KOH contained 0.1 M methanol at a rotating speed of 1600 rpm with a scan rate of 10 mV s^{-1}. As shown in Figure 5**A**, after the methanol was added into the solution, the LSV curve of polyhedral Pd/XC-72 showed a slight decrease in the whole

process. Similarly, Pd/XC-72 (without CTAB, see Figure 5**C**) also kept no dramatic changes in the kinetically controlled regions except a large reduction on limiting current density. In contrast, the ORR polarization curves of Pd/XC-72 (without Fe^{3+}, see Figure 5**B**) and commercial Pd/C (see Figure 5**D**) appeared a significant methanol oxidation peaks in the ORR polarization curves, while their half-wave potential shifted more negative and the corresponding limiting current densities were also greatly reduced. These results could be ascribed to the competition between methanol oxidation and O_2 reduction on the surface of Pd, thus resulted a strong interference in the process of ORR.[56,57] Thus, the together introduced Fe^{3+} and CTAB into the precursors are necessary and very important because they could greatly improve the electrocatalytic ORR performance as well as increasing the methanol tolerance ability simultaneously.

The long-term durability of a designed cathode catalyst is an important criterion for practical fuel cells application as well. Figure 6 presents the chronoamperometric curves of polyhedral Pd/XC-72 and commercial Pd/C at -0.4 V in O_2-saturated 0.1 M KOH solution with 1600 rpm for 7200 s. It can be found that the current densities of the two catalysts decrease rapidly in the initial period, and then slowly reach a relative stable stage. From the resulted relative current, the polyhedral Pd/XC-72 displays a more stable curve with lost ca. 40% of its initial
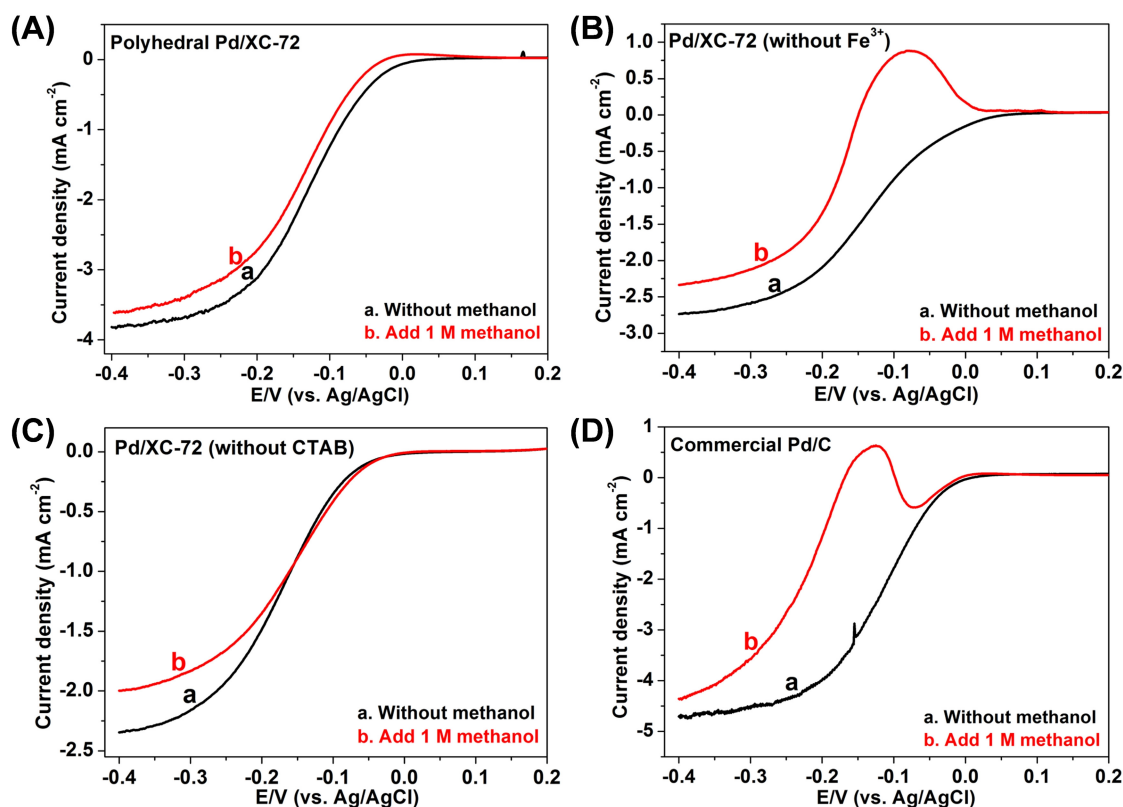
Figure 5. ORR polarization curves of (A) polyhedral Pd/XC-72, (B) Pd/XC-72 (without Fe^{3+}), (C) Pd/XC-72 (without CTAB) and (D) commercial Pd/C in O_2-saturated 0.1 M KOH with and without the presence of methanol at a scan rate of 10 mV s^{-1} and rotation rate of 1600 rpm.
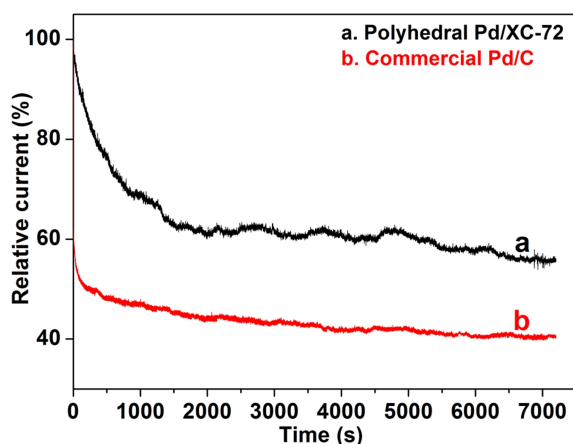

Figure 6. Long-term stability testing for (a) polyhedral Pd/XC-72 and (b) commercial Pd/C in O_2-saturated 0.1 M KOH with a rotating speed for 1600 rpm.

activity after continuous running 7200 s. For comparison, the commercial Pt/C endures a dramatic recession and decays about 61% of its initial activity under the same experimental conditions. The slower deterioration of polyhedral Pd/XC-72 could be ascribe to that the special structures of Pd crystal could mitigate the Ostwald ripening and consequently restrains

undesirable agglomeration of Pd particles, thus improving the ORR stability of polyhedral Pd/XC-72 catalyst.[58]

Conclusion

In summary, polyhedral Pd nanocrystals are successfully prepared by a facile one-pot hydrothermal synthetic method using CTAB and $FeCl_3$ as structural orientation agent and modificative agent. The SEM and TEM images indicate that polyhedral Pd crystals possess a clear hexagonal structure with high surface energy and lots of defects in the presence of CTAB and a small amount of Fe^{3+}. Electrochemical performance shows that the resulted polyhedral Pd/XC-72 catalyst exhibits a more positive onset potential compared to the commercial Pd/C catalyst and presents a higher limiting current density than the compared Pd/XC-72 with only CTAB or Fe^{3+} in the precursor solution. In addition, the electron transfer numbers of polyhedral Pd/XC-72 indicate a four-electron-transfer pathway and the Tafel slope reveals a higher intrinsic activity for ORR. More importantly, the designed polyhedral Pd/XC-72 catalyst has also showed excellent methanol-tolerance crossover effects and long-term stability in alkaline solution. The polyhedral Pd/XC-72 catalyst is expected to be a promising cathode electro-catalyst for portable applications in future DMFC.

Chemistry SELECT ✓ Full Papers

Supporting Information Summary:

All experimental details are provided in the Supporting Information.

Acknowledgements

Conflict of Interest

The authors declare no conflict of interest.

[1] M. R. Gao, Q. Gao, J. Jiang, C. H. Cui, W. T. Yao, S. H. Yu, *Angew. Chem. Int. Ed.* **2011**, *50*, 4905.
[2] J. Luxa, V. Mazánek, M. Pumera, P. Lazar, D. Sedmidubsky, M. Callisti, T. Polcar, Z. Sofer, *Chem.-Eur. J.* **2017**, *23*, 8082.
[3] R. Ning, J. Tian, A. M. Asiri, A. H. Qusti, A. O. Al-Youbi, X. Sun, *Langmuir* **2013**, *29*, 13146.
[4] X. Peng, D. Chen, X. Yang, D. Wang, M. Li, C.-C. Tseng, R. Panneerselvam, X. Wang, W. Hu, J. Tian, Y. Zhao, *ACS Appl. Mater. Interfaces* **2016**, *8*, 33673.
[5] L. Lu, Q. Hao, W. Lei, X. Xia, P. Liu, D. Sun, X. Wang, X. Yang, *Small* **2015**, *11*, 5833.
[6] G. F. Xinyu Liu, Yu Chen, * Yawen Tang, Peiliang She, and Tianhong Lu, *Chem. Eur. J.* **2014**, *20*, 585.
[7] L. An, M. Zhu, B. Dai, F. Yu, *Electrochim. Acta* **2015**, *176*, 222.
[8] Q. Wang, Z. Tang, L. Wang, H. Yang, W. Yan, S. Chen, *ChemistrySelect* **2016**, *1*, 6044.
[9] L. Wang, Z. Tang, W. Yan, H. Yang, Q. Wang, S. Chen, *ACS Appl. Mater. Interfaces* **2016**, *8*, 20635.
[10] Y. Xiong, H. Shan, Z. Zhou, Y. Yan, W. Chen, Y. Yang, Y. Liu, H. Tian, J. Wu, H. Zhang, D. Yang, *Small* **2017**, *13*, 1603423.
[11] H. Yang, Z. Tang, W. Yan, L. Wang, Q. Wang, Y. Zhang, Z. Liu, S. Chen, *J. Alloy. Compd.* **2017**, *702*, 146.
[12] H. Yang, C. Wen, Z. Tang, L. Wang, Q. Wang, W. Yan, W. Wu, S. Chen, *J. Mater. Sci.* **2017**, *52*, 8016.
[13] G. Jiang, H. Zhu, X. Zhang, B. Shen, L. Wu, S. Zhang, G. Lu, Z. Wu, S. Sun, *ACS Nano* **2015**, *9*, 11014.
[14] N. Zhang, Y. Feng, X. Zhu, S. Guo, J. Guo, X. Huang, *Adv. Mater.* **2016**, *29*, 1603774.
[15] K. Sasaki, H. Naohara, Y. Choi, Y. Cai, W.-F. Chen, P. Liu, R. R. Adzic, *Nat. Commun.* **2012**, *3*, 1115.
[16] Y. Lu, Y. Jiang, X. Gao, X. Wang, W. Chen, *J. Am. Chem. Soc.* **2014**, *136*, 11687.
[17] J. Zhang, X. Yang, H. Shao, C.-C. Tseng, S. Tian, W. Hu, C. Jing, J. Tian, Y. Zhao, *Fuel Cells* **2017**, *17*, 115.
[18] H.-S. Chen, Y.-T. Liang, T.-Y. Chen, Y.-C. Tseng, C.-W. Liu, S.-R. Chung, C.-T. Hsieh, C.-E. Lee, K.-W. Wang, *Chem. Commun.* **2014**, *50*, 11165.
[19] D. Liu, Q. Guo, H. Hou, O. Niwa, T. You, *ACS Catal.* **2014**, *4*, 1825.
[20] W. Yan, Z. Tang, L. Li, L. Wang, H. Yang, Q. Wang, W. Wu, S. Chen, *ChemElectroChem* **2017**, *4*, 1349.
[21] G.-R. Xu, F.-Y. Liu, Z.-H. Liu, Y. Chen, *J. Mater. Chem. A* **2015**, *3*, 21083.
[22] S. Guo, S. Zhang, D. Su, S. Sun, *J. Am. Chem. Soc.* **2013**, *135*, 13879.
[23] V. Paunovic, V. Ordomsky, M. Fernanda Neira D'Angelo, J. C. Schouten, T. A. Nijhuis, *J. Catal.* **2014**, *309*, 325.
[24] J.-J. Feng, D.-L. Zhou, H.-X. Xi, J.-R. Chen, A.-J. Wang, *Nanoscale* **2013**, *5*, 6754.
[25] R. Zhao, M. Gong, H. Zhu, Y. Chen, Y. Tang, T. Lu, *Nanoscale* **2014**, *6*, 9273.
[26] J.-N. Zheng, M. Zhang, F.-F. Li, S.-S. Li, A.-J. Wang, J.-J. Feng, *Electrochim. Acta* **2014**, *130*, 446.
[27] J.-J. Lv, N. Wisitruangsakul, J.-J. Feng, J. Luo, K.-M. Fang, A.-J. Wang, *Electrochim. Acta* **2015**, *160*, 100.
[28] Y.-F. Li, J.-J. Lv, M. Zhang, J.-J. Feng, F.-F. Li, A.-J. Wang, *J. Electroanal. Chem.* **2015**, *738*, 1.
[29] Y. Qi, J. Wu, H. Zhang, Y. Jiang, C. Jin, M. Fu, H. Yang, D. Yang, *Nanoscale* **2014**, *6*, 7012.
[30] L.-M. Chen, Y.-N. Liu, *CrystEngComm* **2011**, *13*, 6481.
[31] N. Zhang, Y. Deng, Q. Tai, B. Cheng, L. Zhao, Q. Shen, R. He, L. Hong, W. Liu, S. Guo, K. Liu, H.-R. Tseng, B. Xiong, X.-Z. Zhao, *Adv. Mater.* **2012**, *24*, 2756.
[32] M. Jin, H. Zhang, Z. Xie, Y. Xia, *Energy Environ. Sci.* **2012**, *5*, 6352.
[33] J. Bai, L. Shen, D. Sun, Y. Tang, T. Lu, *CrystEngComm* **2014**, *16*, 10445.
[34] S. Kondo, M. Nakamura, N. Maki, N. Hoshi, *J. Phys. Chem. C* **2009**, *113*, 12625.
[35] X. Yang, M. Zhen, G. Li, X. Liu, X. Wang, C. Shu, L. Jiang, C. Wang, *J. Mater. Chem. A* **2013**, *1*, 8105.
[36] Y. Chen, B. He, T. Huang, H. Liu, *Colloid Surf. A-Physicochem. Eng.* **2009**, *348*, 145.
[37] M. Liu, Y. Lu, W. Chen, *Adv. Funct. Mater.* **2013**, *23*, 1289.
[38] B. Lim, M. Jiang, J. Tao, P. H. C. Camargo, Y. Zhu, Y. Xia, *Adv. Funct. Mater.* **2009**, *19*, 189.
[39] P. Lu, N. Lu, J. Wang, M. J. Kim, Y. Xia, *Nanotechnology* **2014**, *25*, 014003.
[40] B. Huang, L. Chen, Y. Wang, L. Ouyang, J. Ye, *Chem.-Eur. J.* **2017**, *23*, 7710.
[41] Y. Zhao, X. Yang, J. Tian, F. Wang, L. Zhan, *Int. J. Hydrogen Energy* **2010**, *35*, 3249.
[42] H. Li, S. Liao, C. You, B. Zhang, H. Song, Z. Fu, *Int. J. Hydrog. Energy* **2014**, *39*, 14018.
[43] D. Wang, H. L. Xin, Y. Yu, H. Wang, E. Rus, D. A. Muller, H. D. Abruña, *J. Am. Chem. Soc.* **2010**, *132*, 17664.
[44] W. Zhou, J. Y. Lee, *J. Phys. Chem. C* **2008**, *112*, 3789.
[45] Y. Zhao, X. Yang, J. Tian, F. Wang, L. Zhan, *Mater. Sci. Eng. B* **2010**, *171*, 109.
[46] R. N. Singh, A. Singh, Anindita, *Carbon* **2009**, *47*, 271.
[47] S. Zhu, Z. Chen, B. Li, D. Higgins, H. Wang, H. Li, Z. Chen, *Electrochim. Acta* **2011**, *56*, 5080.
[48] Y. Yu, L. Gao, X. Liu, Y. Wang, S. Xing, *Chem.-Eur. J.* **2017**,*23*,10690.
[49] H. Niwa, K. Horiba, Y. Harada, M. Oshima, T. Ikeda, K. Terakura, J.-i. Ozaki, S. Miyata, *J. Power Sources* **2009**, *187*, 93.
[50] M.-H. Shao, K. Sasaki, R. R. Adzic, *J. Am. Chem. Soc.* **2006**, *128*, 3526.
[51] E. Yeager, *J. Mol. Catal.* **1986**, *38*, 5.
[52] A. P. Periasamy, W.-P. Wu, G.-L. Lin, Z.-Y. Shih, Z. Yang, H.-T. Chang, *J. Mater. Chem. A* **2014**, *2*, 11899.
[53] S. Fu, C. Zhu, J. Song, M. Engelhard, B. Xiao, D. Du, Y. Lin, *Chem.-Eur. J.* **2017**, *23*, 10460.
[54] K. Cho, S. H. Han, M. P. Suh, *Angew. Chem. Int. Ed.* **2016**, *55*, 15301.
[55] S. Fu, C. Zhu, J. Song, P. Zhang, M. H. Engelhard, H. Xia, D. Du, Y. Lin, *Nanoscale* **2017**, *9*, 1279.
[56] J. Yang, W. Zhou, C. H. Cheng, J. Y. Lee, Z. Liu, *ACS Appl. Mater. Interfaces* **2010**, *2*, 119.
[57] T. Cochell, W. Li, A. Manthiram, *J. Phys. Chem. C* **2013**, *117*, 3865.
[58] R. Zhao, Y. Liu, C. Liu, G. Xu, Y. Chen, Y. Tang, T. Lu, *J. Mater. Chem. A* **2014**, *2*, 20855.